DOI 10.4430/bgo00366

Electrical image logs interpretation from Wenchuan earthquake Fault: Scientific Drilling project-hole4 (WFSD-4)

A.A. Konaté[1], H. Ma[2], H. Pan[2] and N. Khan[2]

[1] *Laboratoire de Recherche Appliquée en Géoscience et Environnement, Institut Supérieur des Mines et Géologie, Boké, Republic of Guinea*

[2] *Institute of Geophysics and Geomatics, China University of Geosciences, Wuhan, Hubei, China*

(Received: 28 March 2021; accepted: 28 June 2021; published online: 17 January 2022)

ABSTRACT Borehole imaging is one of the most rapid and accurate methods for gathering *in-situ* geological feature information. The image logging data from WFSD-4 contain a mass of subsurface information, which plays a significant role in improving the understanding of the Presumed Slip Zone (PSZ) in the northern segment of the Yingxiu-Beichuan Fault. Using the electrical image logs with core data, the lithology and the PSZ characterisation were carried out. The results show abundant bedding and oblique fractures in the main lithologies. From the imaging dip interpretation, the bedding development of the 2012-2123-m section tends to be basically unchanged, but the dip angle varies frequently, and is mainly affected by the drag and pull of the fault. From 2123 m to the bottom of the well, the bedding is undeveloped, the formation is fractured seriously and the fracture breccia is obvious at 2190 m. There is a clear change in the strata: the dip angle alters from steep to gentle, and tends to change from north to south. The breakpoint position should be 2190 m, and the 2012-2190-m segment should be the hanging belt of the fault. Electrical images, conventional log as well as core analysis from WFSD-4, indicate that the slip may occur in fault breccia.

Key words: image logging, Wenchuan earthquake, presumed slip zone, WFSD-4, lithology.

1. Introduction

Earthquakes are one of the most dramatic and powerful natural hazards that can cause significant loss of both lives and income. Up to as many as 10,000 people pass away every year owing to seismic activity (Elnashai and Di Sarno, 2008). On 12 May 2008, the Wenchuan earthquake (also known as the Sichuan earthquake) struck China's Sichuan Province. Two major surface ruptures formed during the earthquake, one along the Yingxiu-Beichuan Fault (YBF), over 250 km long, and the other along the Guanxian-Anxian Fault (GAF) for a length of about 80 km (Zheng *et al.*, 2016 and references therein). About 100,000 people lost their lives; more than 360,000 people were injured. In addition, more than 45.55 million people were affected (TRC, 2018). The earthquake happened in a mountainous region. Beichuan and Yingxiu towns, and a huge number of villages, were destroyed or severely damaged. Wenchuan earthquake was the most damaging earthquake in China since the 1976 Tangshan earthquake (Chen and Booth, 2011). Fig. 1 shows the view of the earthquake affected zone. To respond to this catastrophe, the

Chinese government initiated the Wenchuan earthquake Fault Scientific Drilling (WFSD) project boreholes, which entailed the drilling of wells into the YBF and GAF for geophysical logging and core data. Five boreholes (WFSD-1, WFSD-2, WFSD-3, WFSD-3P, and WFSD-4) were drilled along the co-seismic ruptures of the YBF and GAF. Fig. 2a shows the well location scheme of WFSD. WFSD-4, which we examine here, was drilled to a depth of 2273 m through the YBF northern segment fault. It is deeper than the WFSD-3 (1502.30 m), WFSD-2 (1370 m) and WFSD-1 (1201.15 m) holes, Taiwan Chelungpu Drilling Project (TCDP) hole A (2003 m) and TCDP hole B (1352.60 m). Conversely, it is shallower than the San Andreas Fault at Depth (SAFOD) hole (3200 m), which is the deepest land-scientific fault drilling project. The lithological profile of WFSD-4 is represented as follows (Fig. 3): 22.77-333 m and 454-1472 m are the main developments of slates, with interbedded sandstones and sandy mudstone, whereas 333 to 454 m is mainly developed sandstones interbedded with slates. 1472 to 2053 m is mainly developed argillaceous sandstones and sandstones; 2053-2273 m is interpreted as mainly carbonaceous slate lithology interbedded with carbonaceous sandstones, argillaceous sandstones, sandstones. WFSD is an important scientific project for studying earthquake faults. It is a major scientific measure for earthquake prevention and disaster reduction.

Drilling a well into the fault zone provides a window for earthquake investigations. Geophysical well logging involves measuring the physical properties of adjacent rocks with a sensor located

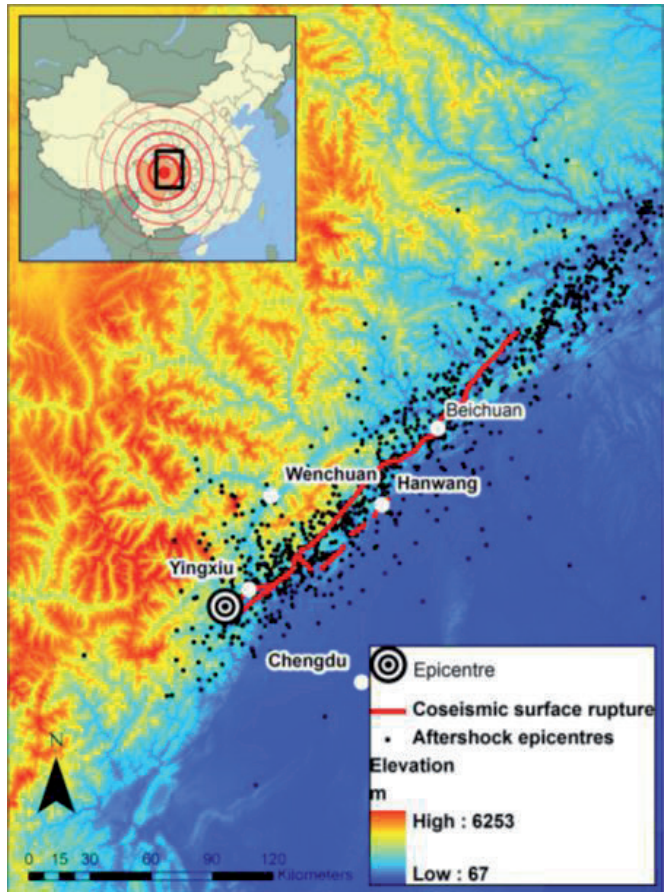

Fig. 1 - Overview of the earthquake affected zone (after Whadcoat, 2011).

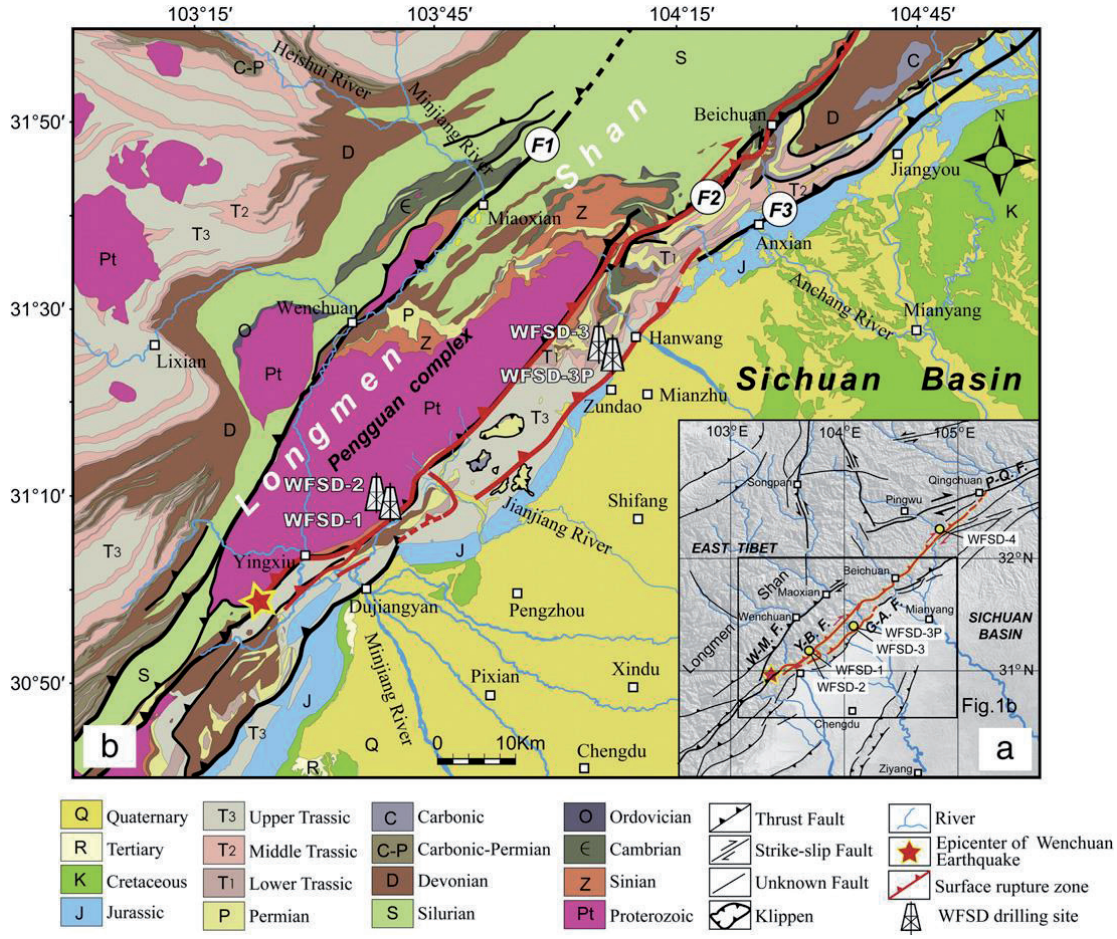

Fig. 2 - Well location scheme of WFSD (a) and geological setting of study area (b). F1: Wenchuan-Maoxian Fault (WMF); F2: Yingxiu-Beichuan Fault (YBF); F3: Guanxian-Anxian Fault (GAF); Pingwu-Qingchuan Fault (PQF) (after Li *et al.*, 2013). Wenchuan earthquake surface rupture zone (red line). WFSD-1 and WFSD-2 are situated in the southern segment of YBF; WFSD-3 and WFSD-3P are sited in the GAF; WFSD-4 is located in the northern segment of YBF.

in a well. Geophysical well logging has played a vital part in the investigation of active fault zones (Yeh *et al.*, 2007; Matsuda *et al.*, 2008; Wu *et al.*, 2008; Hung *et al.*, 2009; Jeppson *et al.*, 2010; Zoback *et al.*, 2011; Kinoshita *et al.*, 2014; Pei *et al.*, 2014; Massiot *et al.*, 2018; Jeppson and Tobin, 2020). Considerable effort has been undertaken by geoscientists to understand the slip behaviour of the Wenchuan earthquake fault (Li *et al.*, 2013, 2014, 2015; Nie *et al.*, 2013; Yang *et al.*, 2013; Lei *et al.*, 2014; Duan *et al.*, 2015; Zheng *et al.*, 2016; Deng *et al.*, 2017; Konaté *et al.*, 2017a, 2017b; Fang *et al.*, 2018, 2020). Despite the huge quantity of studies, there is still no full understanding of the geological features of the Wenchuan earthquake fault. Therefore, this study is an attempt to improve our understanding of the geological features in the northern segment of YBF using borehole imaging data.

Borehole imaging is one of the most rapid and accurate methods for gathering subsurface data. Imaging logging technology uses sensor array scanning or rotating scanning measurement downhole to collect a large amount of information on the formations along the longitudinal, circumferential, and radial directions of the well, in order to obtain an image of the well wall or around the wellbore.

Imaging logging technology has excellent vertical resolution, and the instrument itself has a positioning system, which can describe in detail the geological features such as fractures, faults, and bedding in the formation. Borehole imaging has been and continues to be used as an established technology in fault/fracture zone studies in earthquake science. For instance, Nie *et al.* (2012, 2013) and Zou *et al.* (2012) based on the WFSD-1, WFSD-2, and WFSD-3 holes, investigated fractures and *in-situ* stress direction from borehole image logs and core data. Massiot *et al.* (2018) used ultrasonic image logs obtained from the DFDP-2B borehole in order to describe the continuous record of foliation and fractures in the hanging wall of the central Alpine Fault, New Zealand. Iturino *et al.* (2001) combined downhole images and core data to interpret the San Andreas Fault zone. The TCDP borehole images, combined with a suite of conventional geophysical log and core data, were instead analysed by Wu *et al.* (2007), Wu *et al.* (2008) established the relationships between deformation structures and *in-situ* stress, and identified the Chi-Chi earthquake slip zone. The general understanding collected from the above development is that ultra-high-resolution images associated with conventional log and core data are well suited for earthquake studies. The present study focused on the formation micro-resistivity scanning imaging logging data and core data obtained from the WFSD-4 hole in the northern segment of YBF. The total length of the well processed by imaging logging in WFSD-4 is 22-2268 m, totalling 2246 m. Lithology image feature analysis and description of fracture zone characteristics have been carried out. Furthermore, we discussed the location of the Presumed Slip Zone (PSZ). This study shows that image logs bring another dimension to understanding the geological features of an earthquake. The information gained from the WFSD wells would contribute to earthquake science in general and help improve China's readiness in the event of earthquake disasters.

2. Geological setting of study areas

A powerful earthquake occurred along the Longmenshan Fault belt situated at the transition zone between the border of the Tibetan Plateau and the Sichuan basin (Li *et al.*, 2015 and references therein). Fig. 2b shows the geological setting of the Longmenshan Fault and its adjacent area. Referring to Li *et al.* (2013 and reference therein), the Longmenshan Fault zone is the easternmost thrust belt of the Songpan-Ganzi orogen and is essentially composed of three thrust faults: the YBF, Wenchuan-Maoxian Fault (WMF), and GAF. Additionally, the Longmenshan area can be divided into four parts from west to east: Paleozoic metamorphic terrain, Precambrian metamorphic complexes, Jurassic foreland basin, and Triassic coal-bearing strata. An early Cretaceous ductile detachment belt developed along the WMF (detachment along the eastern margin of the Tibetan plateau), yielding the tectonic extrusion of the Pengguan and Baoxing complexes. The Longmenshan Fault zone is described by thrust sinistral strike-slip motion from late Triassic to Paleogene and by thrust-dextral strike-slip motion since the Meso-Cenozoic. The Longmenshan Fault zone has long been active and its currently active faults have developed along the former faults since the late Triassic (Li *et al.*, 2013). GPS measurements show a very slow deformation rate at a 10-yr scale with less than 2 mm/yr, indicating that the Longmenshan Fault zone has been locked, with a rather long recurrence interval for $M_S \geq 7.0$ earthquakes (~3,000-6,000 years). Certainly, no earthquake larger than M_S 7.0 has occurred along the Longmenshan Fault zone. Note that several M_S 6.0-6.5 seismic events struck along the Longmenshan Fault zone south central segment, and in addition to the north, two events occurred in the Minshan region, namely the 1933 M_S 7.5 Diexi earthquake and the 1975 M_S 7.2 Songpan earthquake. This indicates that there was a reasonably long calm period before

the Wenchuan earthquake struck, with energy accumulation increasing the possibility of large earthquake occurrence (Li *et al.*, 2013). Complete offsets investigation displays two peaks along the YBF, with Qingping town (Mianzhu city) being the boundary. To the south, the maximum vertical displacement is 6.0-6.7 m in Shenxigou and Bajiaomiao villages (Hongkou county), while at Beichuan, the maximum vertical offset is 11-12 m at Shaba village (Qushan county). The two segments commonly correspond to two rupture processes shown by seismic wave inversion. The north is almost purely dextral strike-slip, while the south is a thrust with some dextral strike-slip motion (Li *et al.*, 2013).

3. Data and methodology

WFSD-4 geophysical borehole imaging logging measurements were carried out using the Halliburton's EXCELL-2000 system. The imaging downhole tools include: formation micro-resistivity scanning imaging logging (XRMI) and ultrasonic imaging logging (CAST).

Judging from the processed images, the quality of the electrical images in the entire measurement well section was good, which can accurately reflect the formation conditions; while the quality of the acoustic imaging measurements was average, and the image characteristics were not very obvious. The electrical imaging was clearer and the geological features were obvious, which can meet the needs of interpretation.

Electrical image logs, which are of great importance in geological feature analysis, were investigated at the following depth intervals: 22.77-513.02 m, 501.73-1300.84 m, 1300.84-1444.55 m, 1400-1980 m, and 1972.3-2273 m.

A total of 150 microelectrodes are installed on the 6 polar plates of the XRMI borehole micro-resistivity imaging logging tool, each electrode is 0.2 inch in diameter, and the electrode spacing is 0.1 in. During the measurement, the electrode plate is pushed against the rock of the borehole wall, and the ground instrument vehicle controls the current to be emitted into the formation. The intensity of the current emitted by each electrode varies with the rock and the condition of the borehole wall against which it abuts. Therefore, the recorded current intensity of each electrode and the applied voltage reflect the change of the micro-resistivity around the well wall. A sample is taken every 0.1 inch along the well wall to obtain the small resistivity change of the whole well section.

The dense sampled data, then, undergoes a series of correction processing, such as depth correction, speed correction, etc., the resistivity image can easily be formed; that is, a gradual colour plate or grey scale is used to change the value of each electrode. Each sampling point becomes a colour element. The commonly used colour palettes are black-brown-yellow-white, divided into 42 colour levels, which represent the change in resistivity from low to high. Therefore, subtle changes in colour represent changes in lithology and physical properties.

Data processing is required in order to transform the raw acquisition data from micro-resistivity curves measured by each electrode into a visual representation or an image (Rider, 1996; Grace and Newberry, 1998). The imaging logging data was processed and analysed by Shengli Logging Company using Schlumberger's Geoframe software and LogVision program.

There are many similarities between electrical imaging interpretation and core description, including sedimentary structure, diagenesis phenomenon, lithofacies, structure and fracture, pore analysis, etc. The difference is that imaging logging is a description of the borehole wall, the induced fractures and damage on the borehole wall reflect the influence of ground stress, and the orientation data of bedding and fractures is also difficult to obtain on the core. Of course, the

core is a direct sampling of the underground rock formation, which is the most accurate data. After the two are calibrated, the formation description will be more accurate.

3.1. Lithology image feature analysis

Lithology is one of the main factors influencing the development of fault zones. It can be interpreted using high-resolution micro-resistivity images of the borehole wall (Yuan *et al.*, 2017, and reference therein). Here, after careful observation of cores, downhole electrical images were exploited to characterised lithology. In WFSD-4, most fault zones are developed on carbonaceous slate and carbonaceous sandstone (see Fig. 3). Combined with the core analysis data, the image characteristics of the main lithologies of the well are summarised as follows.

Fig. 4 shows sandstone and carbonaceous sandstone electrical image and core rock sample, respectively. From Fig. 4, sandstone exposed the development of bedding with massive features and the compact lithology. The carbonaceous sandstone demonstrated undeveloped bedding and the colour is dominated by a dark colour and the broken blocks are bright with high resistance and patchy. Again from Fig. 4, the core rock of carbonaceous sandstone is broken along the bedding, and the diagonal fractures of cut bedding are developed.

Carbonaceous slate is the most common lithology in WFSD-4 (see Fig. 3). Fig. 5 illustrates slate and carbonaceous slate electrical image and core rock sample, respectively. From Fig. 5, it can be seen that the bedding is developed on the electrical imaging, and the bedding is finer than that of the sandstone. Because of the carbon content, the carbonaceous slate is more brittle and fragile. The small pieces of broken rock are observable on the core photo (Fig. 5b), displaying high resistance on electrical imaging. From conventional logs (Fig. 6), RD log values are lower in carbonaceous sandstones and carbonaceous slates than that of slates and sandstones. This suggests that carbonaceous slate and carbonaceous sandstone show little resistance. The YBF zone lies in carbonaceous silt-slate, principally composed of fault gouge and fault breccia (Li *et al.*, 2019). Carbonaceous material was also observed at the surface and/or in cores recovered from other WFSD drilling sites (Yang *et al.*, 2013; Kuo *et al.*, 2014, 2018; Li *et al.*, 2015; Liu *et al.*, 2016). Besides, it was also recognised abundantly in drill cores of TCDP (Hirono *et al.*, 2015). This indicates that carbonaceous material is commonly studied to understand fault slip behaviours during earthquakes. Again from Fig. 5, the bedding development on slate is often a group of parallel or nearly parallel conductivity anomalies, and the width of the anomalies is narrow and uniform, very regular, usually low angle or horizontal. The slate bedding is clearer, whereas the carbonaceous slate bedding surface is more obscure. From the point of view of conventional logs curves, evidence can be observed from Fig. 6.

Carbonaceous sandstones are characterised by a high GR value (159.470 API), relatively high DEN value (2.7849 g/cm^3), moderate AC value (61.610 μs/ft), moderate Pe value (5.576 b/e), low RD value (34.324 Ω·m), high SP value (61.177 mV), relatively high K value (3.0581%), relatively high Th value (11.483 ppm), moderate U value (7.387 ppm) and moderate CNL value (11.397%).

Sandstones show a low GR value (99.812 API), moderate DEN value (2.684 g/cm^3), moderate AC value (60.769 μs/ft), moderate Pe value (3.812 b/e), relatively high RD value (314.998 Ω·m), moderate SP value (41.0690 mV), moderate K value (2.125%), moderate Th value (7.68 ppm), moderate U (5.288 ppm) and relatively low CNL value (8.923%).

Carbonaceous slates show a high GR value (174.393 API), moderate DEN value (2.7121 g/cm^3), moderate AC value (59.906 μs/ft), moderate Pe value (6.284 b/e), low RD value (54.986 Ω·m), high SP value (84.377 mV), relatively high K value (3.309%), high Th (12.045 ppm), moderate U value (7.983 ppm) and high CNL value (17.290%)

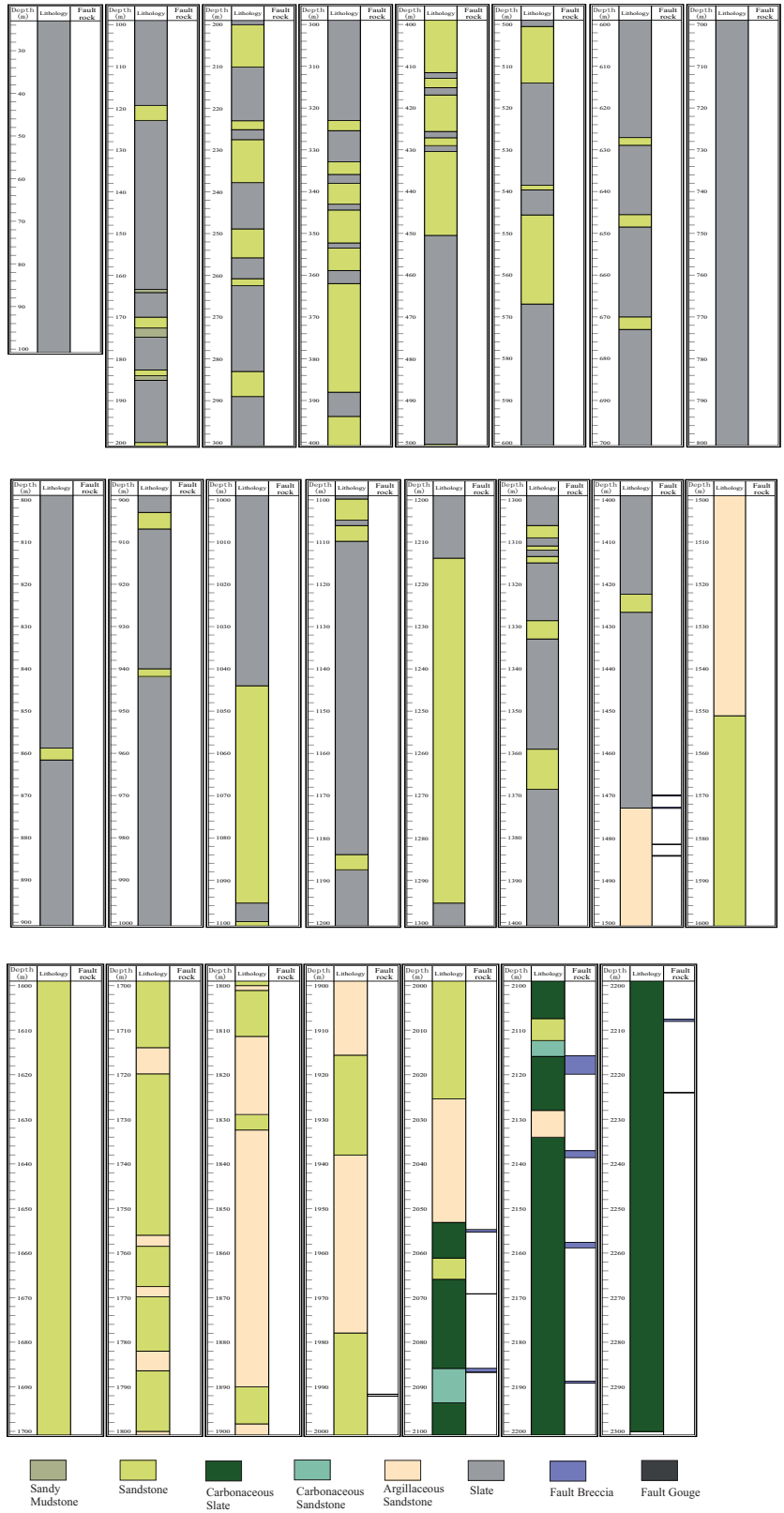

Fig. 3 - Lithological profile (original rock) and fault rock distribution of the WFSD-4 cores, with depth being the well depth.

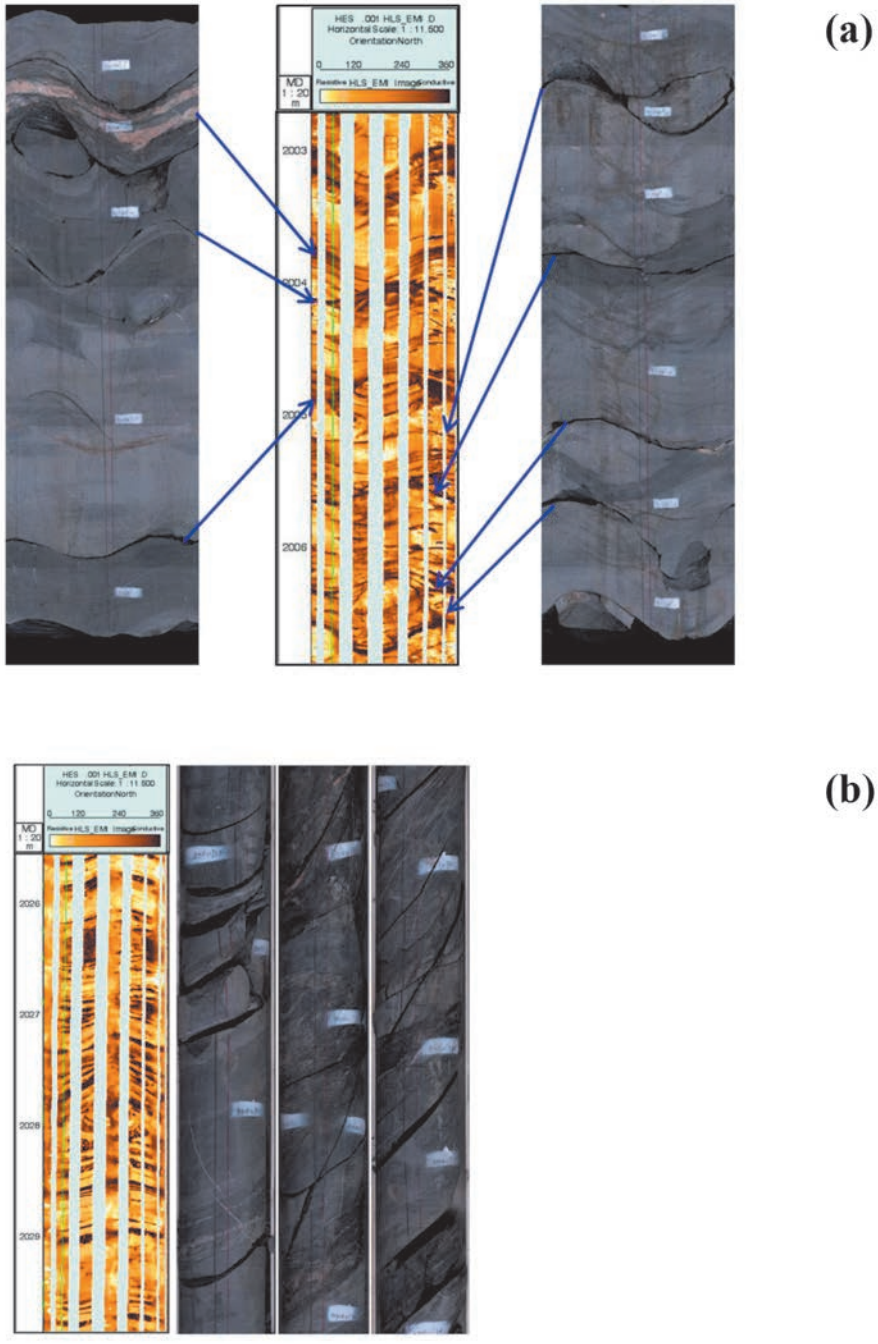

Fig. 4 - A section of WSFD-4 well electrical image and core rock sample. Depth scale is in metres: a) sandstone; b) carbonaceous sandstone.

Slates are characterised by a moderate GR value (116.170 API), moderate DEN value (2.682 g/cm^3), moderate AC value (64.053 µs/ft), moderate Pe value (4.2075 b/e), moderate RD value (235.356 Ω·m), moderate SP value (39.457 mV), moderate K value (2.3406%), moderate Th (9.123 ppm), moderate U (6.370 ppm) and moderate CNL value (12.123%).

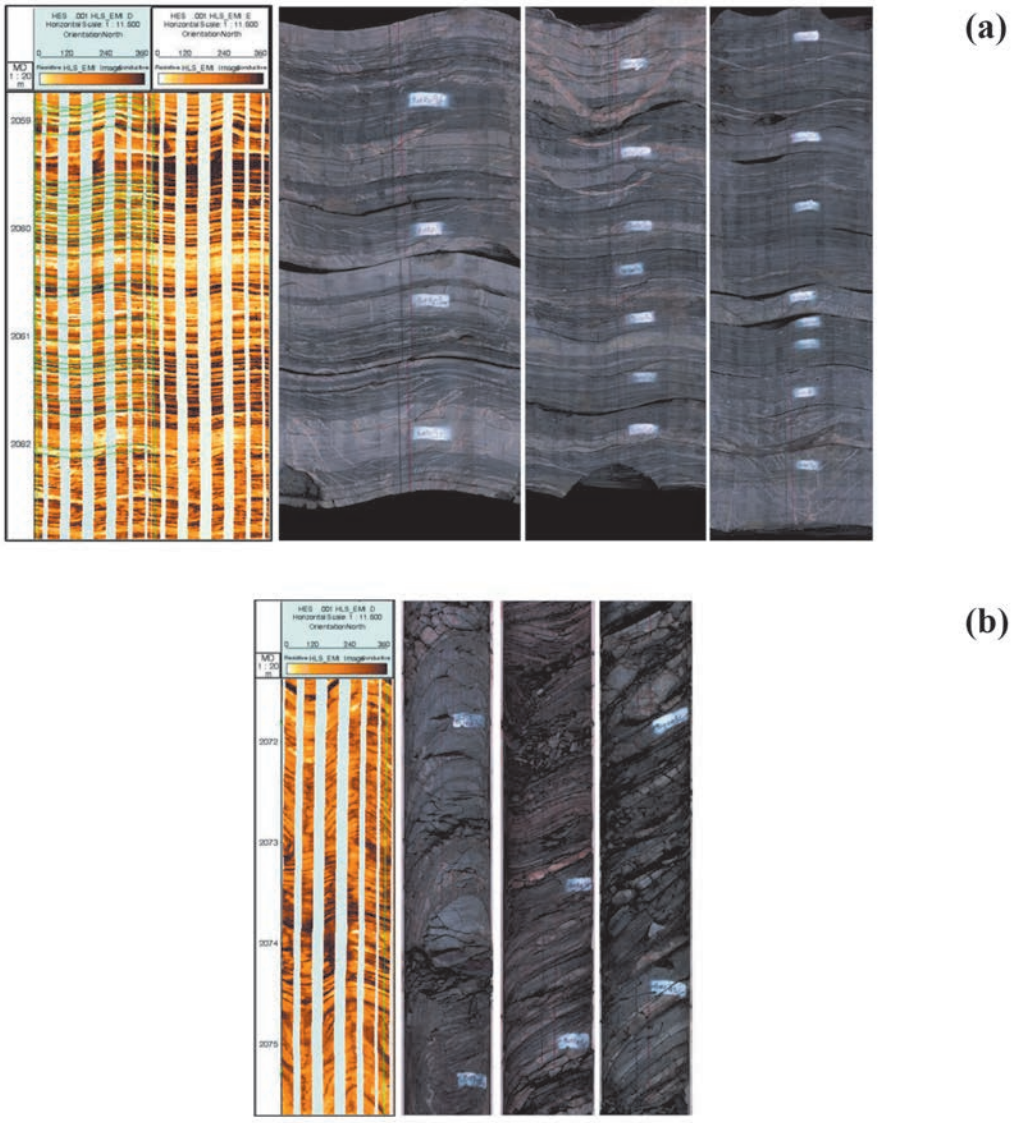

Fig. 5 - A section of WSFD-4 well electrical image and core rock sample. Depth scale is in metres: a) slate; b) carbonaceous slate.

4. Description of fracture zone

Fractures are surfaces of brittle mechanical failure in a rock. As mentioned by Deng *et al.* (2017), the WFSD wells display many fractures, including natural fractures and induced fractures, and high dip-angle conductive fractures are the most common fractures. Fig. 7 shows the fracture imaging of WFSD-4. There are factures in the imaging measurement section of WFSD-4, mainly high-conductivity fractures. The image features are low-resistance dark sinusoidal fringe curves. The fracture surface is clear and the dissolution phenomenon is generally not developed in rock samples. Generally speaking, the distribution of fracture angles is wide, with medium and high angles being the main ones. In Fig. 7b, high-angle fractures appear as high-amplitude sinusoidal fringe curves on the image, and the angles of individual fractures are nearly vertical. Instead,

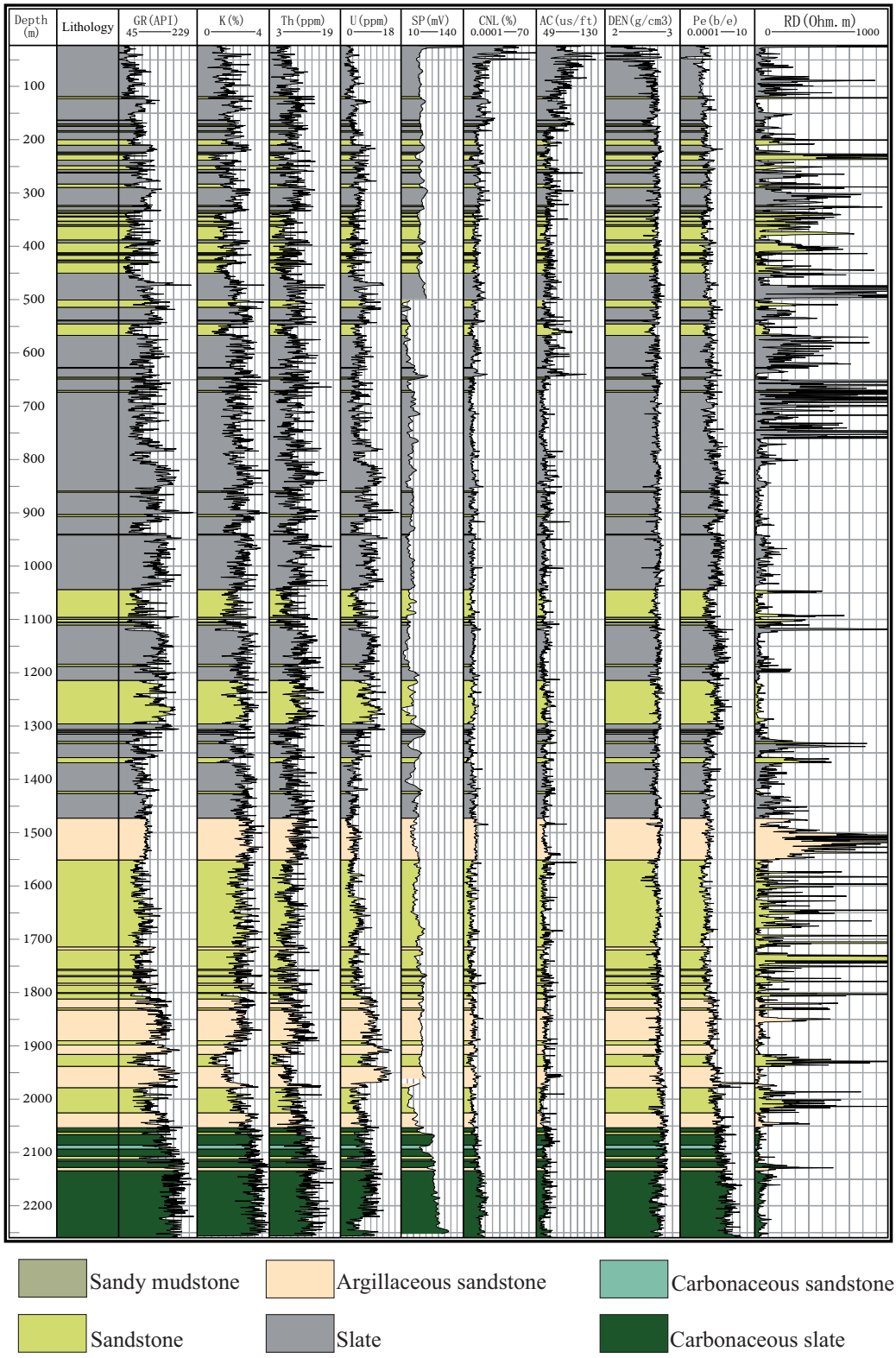

Fig. 6 - Conventional log responses in lithological units from WFSD-4. Variations in physical properties are revealed by the conventional logs.

in Fig. 7a, medium-angle fractures appear on the image. This is a sinusoidal fringe curve with medium amplitude, some will cut through the bedding, and some fractures are parallel to the bedding, and the core shows that bedding fractures occur.

WFSD-4 sections with concentrated fractures are as follows: 226-252 m, 325-329 m, 580-592 m, 605-629 m, 656-700 m, 1248-1258 m, 1330-1343 m, 1363-1417 m, 1440-1575 m, 1575-1620 m, 1687-1702 m, 1920-1938 m, 1983-2011 m, 2044-2053 m, and 2139-2155 m.

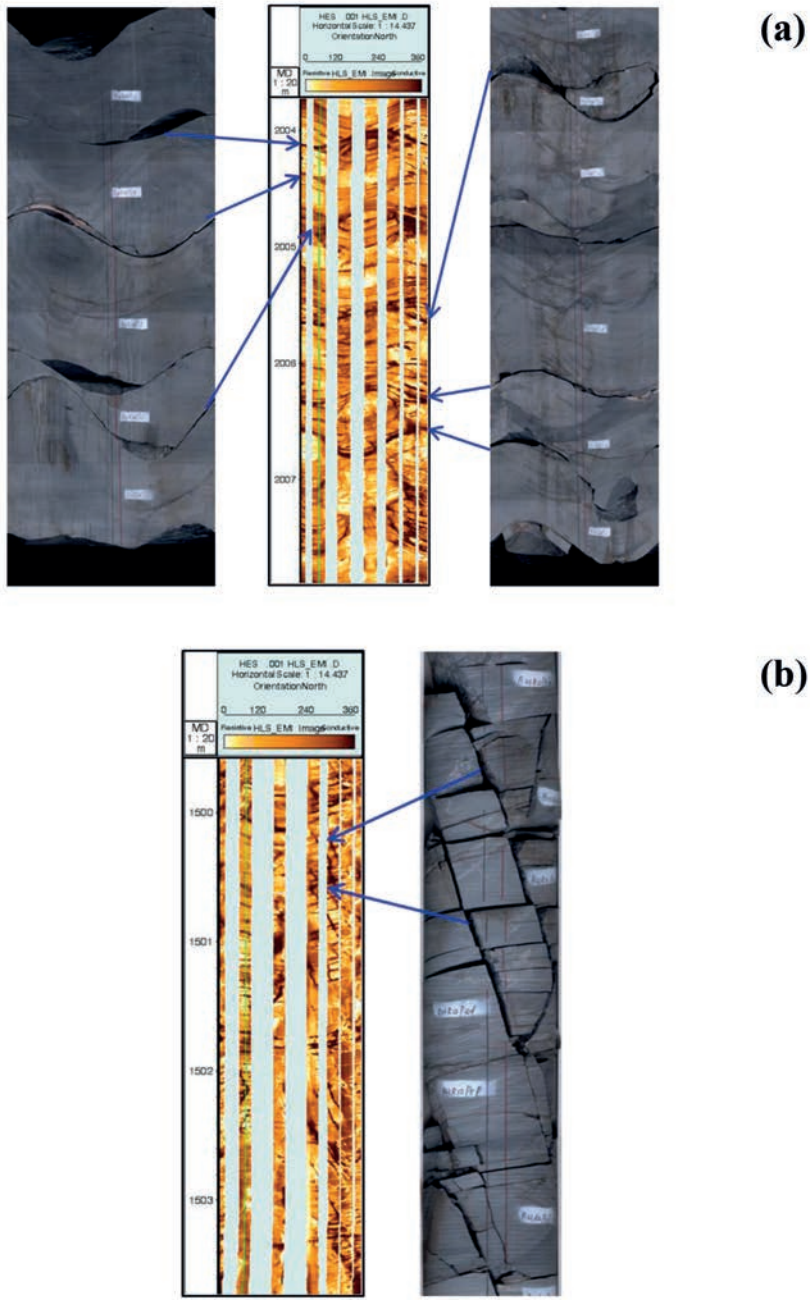

Fig. 7 - Fracture imaging of WFSD-4: a) bedding fractures; b) oblique fractures. Depth is scaled in metres.

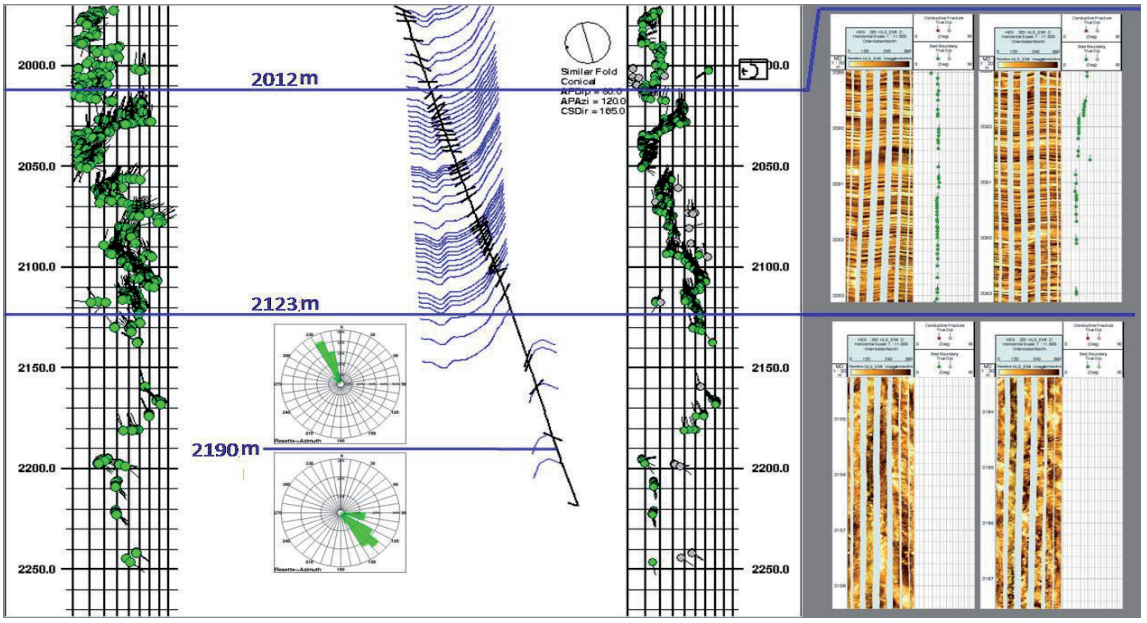

Fig. 8 - Structural cross-section from analysis of bedding dip angle and direction measured by XRMI imaging logging. The cross-section direction is 165° from north. Depth is scaled in metres.

4.1. Main fault zone analysis

According to the imaging dip interpretation, the PSZ of the YBF northern segment may be located between 2012 and 2265 m and the breakpoint may be located around 2190 m (Fig. 8). From Fig. 8, the bedding development of 2012-2123 m section tends to be basically unchanged, but the dip angle varies frequently, and is mainly affected by the drag and pull of the fault. From 2123 m to the bottom of the well, the bedding is undeveloped, the formation is fractured heavily and the fracture breccia is clear at 2190 m. The occurrence of strata has an evident change, the dip angle changes from steep to gentle, and tends to change from north to south. 2190 m should be the breakpoint position and the 2012-2190-m segment should be the hanging belt of the fault.

The features of electrical imaging in fault breccia in the well section are as follows: broken blocks are high resistance, bright colour spots and patches, and their particle sizes are obviously larger than those of other lithologies mentioned above. In addition, fine breccia or ground rock filled between blocks are characterised by low resistivity. Some gravels obviously retain the laminae before breaking, and some are flattened and distributed in layers (Fig. 9). Fault breccia is a potential seismic indicator of fault slip and have been identified in YBF at surface outcrops and/or in cores retrieved from WFSD drilling sites (Yang *et al.*, 2012; Wang *et al.*, 2014; Zhang *et al.*, 2015; Li *et al.*, 2019).

From the point of view of conventional logs, the PSZ of YBF northern segment may be situated between 2012 and 2265 m. Because the electrical resistivity log curve shows the lower values and the gamma ray log curve displays the higher values at a depth of 2012-2265 m as compared to other faults zones in the well (see Konaté *et al.*, 2017a, Fig. 4), among all fault zones, the slip on the 2008 Wenchuan Fault may be localised in the fault zone, FZ2207, which is in between 2207.51 and 2208.04 m depth in carbonaceous slate rock and composed of fault breccia. Fig. 10 shows the conventional log responses in the fault zone FZ2207.

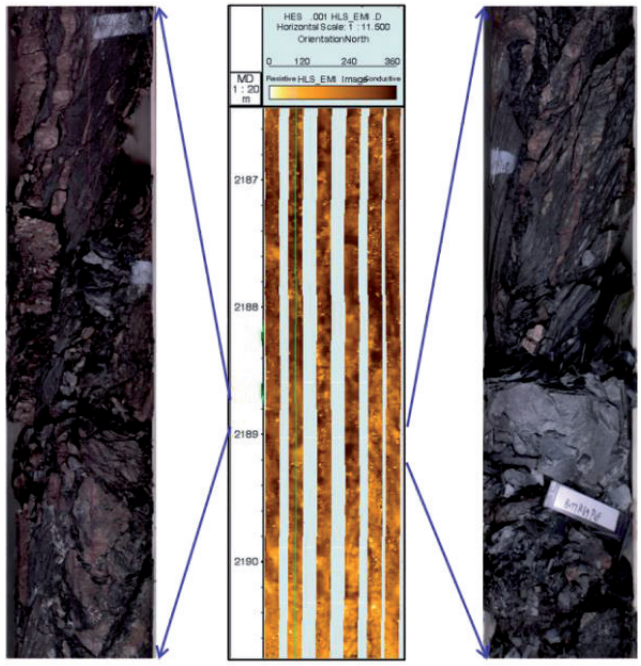

Fig. 9 - The features of electrical imaging in fault breccia. Depth is scaled in metres.

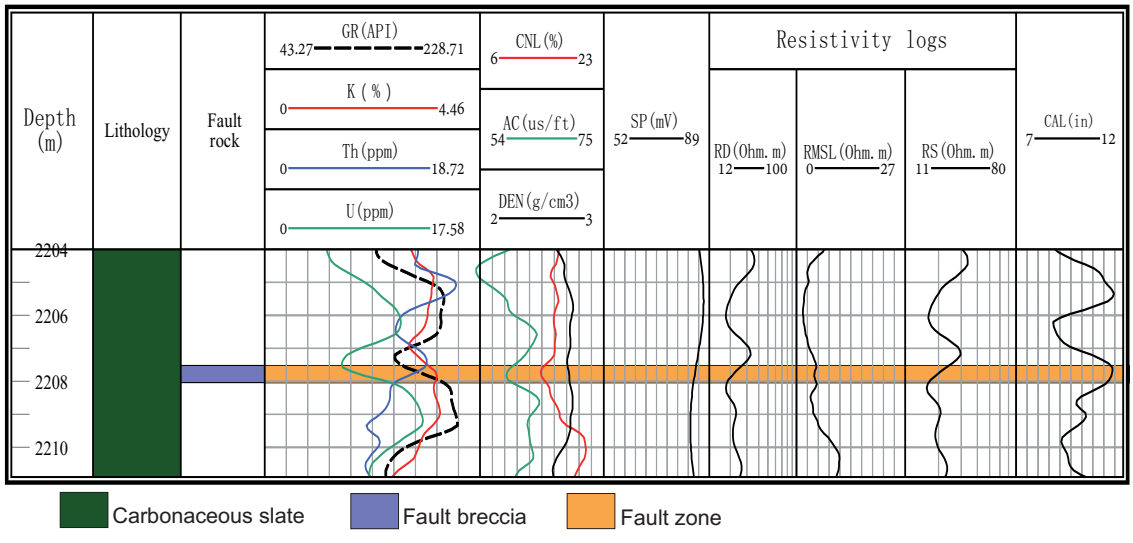

Fig. 10 - Conventional log responses in the fault zone FZ2207 (2207.51-2208.04 m depth). CAL displays a deflection one, RD changes from 32.93 to 17.69 Ω·m with the decrease of RMSL and RS, followed by an increasing trend of CNL. The GR shows a step increase and good agreement with K, Th, and U; as the AC increases, the SP exhibits reduced deflection, there is no obvious change in DEN in the fault zone, however there is a trend towards a slight increase of DEN values with depth.

In addition, from the inspection of the WFSD-4 cores in Fig. 3, the depth interval 2012-2265 m consists of a continuous fault zone with fault breccia of different scale and very few fault gouges. For this reason, we concur that the depth interval 2012-2265 m represents a large-scale fault zone.

Based on the above findings, the consensus is that the slip of the YBF northern segment took place in fault breccia. Additional investigations on physical, mechanical, and chemical properties from surface and laboratory studies of the fault cores, should be made to help recognise the break point. These make it a challenge to correlate earthquakes to specific faults.

5. Conclusions

XRMI imaging logging provides electronic images of the well wall acquired by measuring the resistivity variation of the rocks. Combined with the core analysis data, the image characteristics of the main lithology of WFSD-4 show an abundance of bedding and oblique fractures in the main lithologies. From the imaging dip interpretation, the bedding development of the 2012-2123-m section tends to be basically unchanged, but the dip angle varies frequently, and is mainly affected by the drag and pull of the fault. From 2123 m to the bottom of the well, the bedding is undeveloped, the formation is fractured heavily and the fracture breccia is obvious at 2190-m. The occurrence of strata has an obvious change, the dip angle changes from steep to gentle, and tends to change from north to south. 2190 m should be the breakpoint position and the 2012-2190-m segment should be the hanging belt of the fault.

Electrical images, conventional logs as well as core analyses from WFSD-4, indicate that the slip may occur in fault breccia.

This study shows that image logs add a further dimension to understanding the geological features of an earthquake. The information gained from the WFSD wells would contribute to earthquake science in general, and help improve China's readiness in the event of earthquake disasters.

The research carried out on the WFSD represents progress in understanding slip-weakening effects in the YBF earthquake. However, we still need more data on physical, mechanical, and chemical properties from surface and laboratory studies of the fault cores to fully understand the rupture phenomena of the Wenchuan earthquake fault.

REFERENCES

Chen Y. and Booth D.C.; 2011: *The Wenchuan earthquake of 2008: anatomy of a disaster*. Springer Verlag, Berlin-Heidelberg, Germany, 288 pp., doi: 10.1007/978-3-642-21159-1, ISBN 978-3-642-21159-1.

Deng C., Pan H., Zhao P., Qin R. and Peng L.; 2017: *Fracture modes and identification of fault zones.* In: Abstract, Fall Meeting, American Geophysical Union, New Orleans, LA, USA, #NS33A-0041, Bibcode: 2017AGUFMNS33A0041D.

Duan Q., Yang X., Ma S., Chen J. and Chen J.; 2015: *Fluid-rock interactions in seismic faults: implications from the structures and mineralogical and geochemical compositions of drilling cores from the rupture of the 2008 Wenchuan earthquake, China.* Tectonophys., 666, 260-280.

Fang S., Zhang Z., Wang Z., Pan H. and Du T.; 2020: *Principal slip zone determination in the Wenchuan earthquake Fault Scientific Drilling project-hole 1: considering the Bayesian discriminant function*. Acta Geophys., 68, 1595-1607, doi: 10.1007/s11600-020-00496-z.

Fang Z., Liu Y., Yang D., Guo L. and Zhang L.; 2018: *Real-time hydrogen mud logging during the Wenchuan earthquake Fault Scientific Drilling project (WFSD), holes 2 and 3 in SW China*. Geosci., J 22, 453-464, doi: 10.1007/s12303-017-0068-7.

Grace L.M. and Newberry B.M.; 1998: *Geological application of dipmeter and borehole electrical images*. Unpublished Short Course Notes, Schlumberger Oilfield Services, Houston, TX, USA, v. 8.1.

Hirono T., Maekawa Y. and Yabuta H.; 2015: *Investigation of the records of earthquake slip in carbonaceous materials from the Taiwan Chelungpu Fault by means of infrared and Raman spectroscopies*. Geochem. Geophys. Geosyst., 16, 1233-1253, doi: 10.1002/2014GC005622.

Hung J., Ma K., Wang C. and Ito H.; 2009: *Subsurface structure, physical properties, fault zone characteristics and stress state in scientific drill holes of Taiwan Chelungpu Fault Drilling project.* Tectonophys., 466, 307-321.

Iturino G.J., Goldberg D. and Ketcham R.; 2001: *Integration of core and downhole images in the San Andreas Fault zone*. In: Abstract online, EarthScope Workshop: making and breaking a continent, Snowbird, UT, USA, <www.scec.org/instanet/01news/es_abstracts/Iturrino_et_al.pdf>.

Jeppson T.N. and Tobin H.J.; 2020: *Elastic properties and seismic anisotropy across the Alpine Fault, New Zealand.* Geochem. Geophys. Geosyst., 21, e09073, doi: 10.1016/j.tecto.2020.228410.

Jeppson T.N., Bradbury K.K. and Evans J.P.; 2010: *Geophysical properties within the San Andreas Fault zone at the San Andreas Fault observatory at depth and their relationships to rock properties and fault zone structure*. J. Geophys. Res., 115, B12423, doi: 10.1029/2010JB007563.

Kinoshita M., Gaku Kimura G. and Saito S.; 2014: *Seismogenic processes revealed through the Nankai Trough Seismogenic Zone Experiments: core, log, geophysics, and observatory measurements*. Dev. Mar. Geol., 7, 641-670.

Konaté A.A., Pan H.P., Ma H.L., Qin Z. and Traoré A.; 2017a: *Integrated core-log interpretation of Wenchuan earthquake Fault Scientific Drilling project borehole 4 (WFSD-4)*. Acta Geophys., 65, 683-700, doi: 10.1007/s11600-017-0059-0.

Konaté A.A., Pan H.P., Ma H.L., Qin Z., Bo Guo B., Ziggah Y.Y., Moussounda Kounga C.E., Khan N. and Tounkara F.; 2017b: *Use of spectral gamma ray as a lithology guide for fault rocks: a case study from the Wenchuan earthquake Fault Scientific Drilling project borehole 4 (WFSD-4)*. Appl. Radiat. Isot., 128, 75-85, doi: 10.1016/j.apradiso.2017.06.038.

Kuo L.W., Li H., Smith S.A.F., Di Toro G., Suppe J., Song S-R., Nielsen S., Sheu H-S. and Si J.; 2014: *Gouge graphitization and dynamic fault weakening during the 2008 Mw 7.9 Wenchuan earthquake*. Geol., 42, 47-50.

Kuo L.W., Jyh-Rou Huang J.R., Fang J.N., Si J., Song S-R., Li H. and Yeh E.C.; 2018: *Carbonaceous materials in the fault zone of the Longmenshan Fault belt: 2. Characterization of fault gouge from deep drilling and implications for fault maturity*. Miner., 8, 393, doi: 10.3390/min8090393.

Lei Z., Liu Y., Guo L., Yang D. and Fang Z.; 2014: *Isotope geochemistry of mercury and its relation to earthquake in the Wenchuan earthquake Fault Scientific Drilling project hole-1 (WFSD-1)*. Tectonophys., 619-620, 79-85.

Li C., Li H., Sun Z., Huan W., Zhang L. and Zheng Y.; 2019: *Structural and deformation differences between the northern and southern segments of the Wenchuan earthquake Fault zone, eastern Tibetan plateau*. In: Abstract, Fall Meeting, American Geophysical Union, #MR23E-0169, San Francisco, CA, USA, Bibcode: 2019AGUFMMR23E0169L.

Li H., Wang H., Xu Z., Si J. and Pei J.; 2013: *Characteristics of the fault-related rocks, fault zones and the principal slip zone in the Wenchuan earthquake Fault Scientific Drilling project hole-1 (WFSD-1)*. Tectonophys., 584, 23-42.

Li H., Xu Z., Niu Y., Kong G. and Yao H.; 2014: *Structural and physical property characterization in the Wenchuan earthquake Fault Scientific Drilling project - hole 1 (WFSD-1)*. Tectonophys., 619-620, 86-100.

Li H., Wang H., Yang G., Xu Z., Li T., Si J., Sun Z., Huang Y., Chevalier M-L., Zhang W. and Zhang J.; 2015: *Lithological and structural characterization of the Longmenshan Fault belt from the 3rd hole of the Wenchuan earthquake Fault Scientific Drilling project (WFSD-3)*. Int. J. Earth Sci., 105, 2253-2272, doi: 10.1007/s00531-015-1285-9.

Liu J., Li H., Zhang J. and Zhang B.; 2016: *Origin and formation of carbonaceous material veins in the 2008 Wenchuan earthquake Fault zone.* Earth, Planets and Space, 68, 19, doi: 10.1186/s40623-016-0399-z.

Massiot C., Celerier B., Doan M-L., Tim A., Little T.A., Townend J., McNamara D.D., Williams J., Schmitt D.R., Toy V.G., Sutherland R., Janku-Capova L., Upton P. and Pezard P.A.; 2018: *The Alpine Fault hangingwall viewed from within: structural analysis of ultrasonic image logs in the DFDP2B borehole, New Zealand*. Geochem. Geophys. Geosyst., 19, 2492-2515, doi: 10.1029/2017GC007368.

Matsuda T., Omura K. and Ikeda R.; 2008: *Geological and logging data of the NIED boreholes, Japan, active fault, seismogenic zone, hingeline*. National Research Institute for Earth Science and Disaster Prevention, Tsukuba, Japan, Technical Note, n. 310, 29 pp., ISSN 0917-057X.

Nie X., Zou C.C., Xiao K., Xu J., Niu Y.X. and Kong G.S. ; 2012: *Core spatial position restoring of WFSD-1 borehole with borehole imaging logging data*. Progress in Geophysics, 27, 75–82 (in Chinese with English abstract).

Nie X., Changchun Zou C., Pan L., Huang Z. and Dongming Liu D.; 2013: *Fracture analysis and determination of in-situ stress direction from resistivity and acoustic image logs and core data in the Wenchuan earthquake Fault Scientific Drilling borehole-2 (50-1370 m).* Tectonophys., 593, 161-171.

Pei J., Li H., Wang H., Si J., Sun Z. and Zhou Z.; 2014: *Magnetic properties of the Wenchuan earthquake Fault Scientific Drilling project hole-1 (WFSD-1), Sichuan Province, China*. Earth Planets and Space, 66, 23, doi: 10.1186/1880-5981-66-23.

Rider M.; 1996: *The geological interpretation of well logs, 2nd ed*. Whittles Publishing, Dunbeath, Scotland, UK, 280 pp.

Taiwan Red Cross (TRC); 2018: *10th anniversary of Wenchuan earthquake.* <www.redcross.org.tw/english/home.jsp?pageno=201402140002&acttype=view&dataserno=201805170002>.

Wang H., Li H., Si J., Sun Z. and Huang Y.; 2014: *Internal structure of the Wenchuan earthquake fault zone, revealed by surface outcrop and WFSD-1 drilling core investigation*. Tectonophys., 619-620, 101-114.

Whadcoat S.K.; 2011: *Landsliding and sediment dynamics following the 2008 Wenchuan earthquake in the Beichuan area of China*. Master Thesis in Geological Sciences, Durham University, Durham, UK, 165 pp.

Wu H-Y., Ma K-F., Zoback M., Boness N., Ito H., Hung J-H. and Hickman S.; 2007: *Stress orientations of Taiwan Chelungpu-Fault Drilling Project (TCDP) hole-A as observed from geophysical logs*. Geophys. Res. Lett., 34, L01303, doi: 10.1029/2006GL028050.

Wu Y-H., Yeh E-C., Dong J-J., Kuo L-W., Hsu J-Y. and Hung J-H.; 2008: *Core-log integration studies in hole-A of Taiwan Chelungpu-Fault Drilling Project*. Geophys. J. Int., 174, 949-965, doi: 10.1111/j.1365-246X.2008.03841.x.

Yang T., Chen J., Wang H. and Jin H.; 2012: *Magnetic properties of fault rocks from the Yingxiu-Beichuan Fault: constraints on temperature rise within the shallow slip zone during the 2008 Wenchuan earthquake and their implications*. J. Asian Earth Sci., 50, 52-60.

Yang T., Chen J., Yang X., Wang H. and Jin H.; 2013: *Differences in magnetic properties of fragments and matrix of breccias from the rupture of the 2008 Wenchuan earthquake, China: relationship to faulting.* Tectonophys., 601, 112-124.

Yeh E., Sone H., Nakaya T., Ian K-H., Song S., Hung J-H., Lin W., Hirono T., Wang C-Y., Ma K-F., Soh W. and Kinoshita M.; 2007: *Core description and characteristics of fault zones from hole-A of the Taiwan Chelungpu-Fault Drilling Project.* Terr**.** Atmos. Ocean. Sci., 18, 327-357.

Yuan R., Zhang C., Tang Y., Jianhua Qu J., Guo X., Sun Y., Zhu R. and Zhou Y.; 2017: *Utilizing borehole electrical images to interpret lithofacies of fan-delta: a case study of Lower Triassic Baikouquan formation in Mahu depression, Junggar basin, China*. Open Geosci., 9, 539-553, doi: 10.1515/geo-2017-0041.

Zhang L. Jr., Sun Z., Li H., Cao Y., Ye X., Wang L., Zhao Y. and Han S.; 2015: *Magnetic properties of cores from the Wenchuan earthquake Fault Scientific Drilling hole-2 (WFSD-2), China*. In: Abstract, Fall Meeting, American Geophysical Union, San Francisco, CA, USA, MR33B-2662, Bibcode: 2015AGUFMMR33B2662Z.

Zheng Y., Li H. and Gong Z.; 2016: *Geothermal study at the Wenchuan earthquake Fault Scientific Drilling project-hole 1 (WFSD-1): borehole temperature, thermal conductivity, and well log data.* J. Asian Earth Sci., 117, 23-32.

Zoback M., Hickman S. and Ellsworth W. and SAFOD Science Team; 2011: *Scientific drilling into the San Andreas Fault zone - an overview of SAFOD's first five years*. Scientific Drilling, 11, 14-28, doi: 10.2204/iodp.sd.11.02.2011.

Zou C.C., Liu D.M., Nie X., Xiang B., Niu Y.X. and Kong G.S.; 2012: *Fracture characterization using image logging in Borehole 3 of Wenchuan Earthquake Fault Zone Scientific Drilling (WFSD-3)*. Geoscience, 26, 1146–1153 (in Chinese with English abstract).

Corresponding author: Ahmed Amara Konaté
Laboratoire de Recherche Appliquée en Géoscience et Environnement, Institut Supérieur des Mines et Géologie de Boké
B.P. 84, Boké, Republic of Guinea
Phone: +224 623 359183; e-mail: konate77@yahoo.fr